Toward global inverse solutions for current and past ice mass variations: Contribution of secular satellite gravity and topography change measurements

Xiaoping Wu, Michael M. Watkins, Erik R. Ivins, Ronald Kwok, and Ping Wang
Jet Propulsion Laboratory, California Institute of Technology, Pasadena, California, USA

John M. Wahr
Department of Physics and CIRES, University of Colorado, Boulder, Colorado, USA

Received 2 May 2001; revised 28 February 2002; accepted 4 March 2002; published 14 November 2002.

[1] We investigate the accuracy and resolution of estimating global ice mass variations using secular gravity and ice elevation change observations by the planned Gravity Recovery and Climate Experiment (GRACE) and ICESat missions. The gravity and altimetry data combination can determine the total bedrock uplift rate with root-mean-square (RMS) errors of 0.2–1.3 mm/yr when Gaussian averaged over a half scale of 250 km. Moreover, covariance analyses indicate that the mean snow compaction error can be constrained to the level of 3 mm/yr in equivalent Antarctic ice thickness change. The mean Antarctic present-day ice mass change could then be determined to about 4 mm/yr. For a known viscosity profile, such data sets provide a spatial estimate of a linear combination of the late Pleistocene deglaciation and a more recent past trend (last few thousand years) in the Greenland and Antarctica mass balance. For example, when the linear rate of the recent past trend is estimated solely for ice history, the RMS errors of the 450-km Gaussian averages range between 1 and 3 cm/yr. Although contaminated by the signature of present-day hydrological variations over the deglaciated areas, the 450-km Gaussian-averaged Last Glacial Maximum height of the ancient ice sheets can be determined to a RMS level of 300 m. The mean recovery errors are less than 100 m. However, the gravity/altimeter data cannot resolve the load history and lower mantle viscosity simultaneously. Additional data such as relative sea level records must be invoked to overcome this difficulty. *INDEX TERMS:* 1214 Geodesy and Gravity: Geopotential theory and determination; 1863 Hydrology: Snow and ice (1827); 8122 Tectonophysics: Dynamics, gravity and tectonics; *KEYWORDS:* gravity, inverse, ice, rebound, GRACE, sea level

Citation: Wu, X., M. M. Watkins, E. R. Ivins, R. Kwok, P. Wang, and J. M. Wahr, Toward global inverse solutions for current and past ice mass variations: Contribution of secular satellite gravity and topography change measurements, *J. Geophys. Res.*, *107*(B11), 2291, doi:10.1029/2001JB000543, 2002.

1. Introduction

[2] Assessment of the mass balance state of polar ice sheets is one of the most important challenges faced by glaciologists, since it has far-reaching implications for climatology and society in general. Recently, gravity, crustal motion and Earth orientation signatures due to continental polar ice variations have also attracted attention in the geodetic community [e.g., *Wahr et al.*, 1995; *James and Ivins*, 1998; *Trupin and Shum*, 2001]. Also, radar and laser altimetry have emerged as an important geodetic technique in measuring elevation changes over substantial areas of the great ice sheets with high spatial resolution [*Davis et al.*, 1998; *Krabill et al.*, 1995; *Wingham et al.*, 1998]. A new opportunity will be provided by the Gravity Recovery and Climate Experiment (GRACE) satellite mission and the Geoscience Laser Altimeter System (GLAS) on-board the ICESat mission. Both missions are scheduled for launch into nearly polar orbits in 2002. Gravity and ice topography will be measured, respectively, with high resolution and nearly global coverage over a nominal 5-year mission lifetime.

[3] One of the well-recognized problems in the interpretation of secular gravity and topography change data over Greenland and Antarctica is the separability of the signatures of current and past ice load change. Since the solid Earth deforms viscoelastically, it responds simultaneously to the present-day ice mass imbalance, to late Pleistocene deglaciation, and to any ice mass variations that may have occurred during the last few thousand years. One systematic error source in linking ice altimetry to the mass variation is associated with the poorly constrained viscoelastic bedrock rebound. Another error source is the possible thinning or thickening of the surface snow/firn layer whose density is smaller than fully compacted grains of crystalline ice.

0148-0227/02/2001JB000543$09.00

Although models are available for firn layer evolution [*Arthern and Wingham*, 1998], fluctuations in accumulation or sublimation rates away from steady state are unlikely to be known accurately. The net uncertainty generated by firn evolution is referred to as the compaction error.

[4] *Wahr et al.* [2000] have taken an iterative approach in combining the gravity and altimetry data sets based, in part, upon a linear proportionality between viscous gravity and uplift [*Wahr et al.*, 1995]. The approach would efficiently remove most of the viscous rebound error from the altimeter measurement of the present-day ice mass variation if compaction error were not significant when altimetric measurements are converted to mass variations. They conclude that compaction and under-sampling related errors dominate for a data window as short as 5 years.

[5] The viscoelastic-gravitational response of the Earth to the late Pleistocene melting of the massive ice sheets, commonly referred as postglacial rebound (PGR), has been studied extensively. The modeled ice history and the mantle viscosity profile are largely constrained by relative sea level (RSL) records [e.g., *Peltier and Andrews*, 1976; *Wu and Peltier*, 1983; *Nakada and Lambeck*, 1988; *Mitrovica and Peltier*, 1991a; *Tushingham and Peltier*, 1991]. More recently, geodetic observations have provided additional constraints [e.g., *Yoder et al.*, 1983; *Mitrovica and Peltier*, 1989, 1993; *Milne et al.*, 2001]. However, the characteristics of the various methods used for model construction make it difficult to evaluate both the uncertainty and the space-time resolution for the ice load and mantle viscosity profile. In particular, the RSL data may be more sensitive to total ice volume in certain regions than to the detailed spatial distribution. The inferences from the RSL data may be complicated by their sensitivity to both the space-time history of the ice load and mantle rheology. Non-uniqueness in the inferences can be substantial [e.g., *Nakada and Lambeck*, 1987; *Mitrovica and Peltier*, 1991a, 1991b; *Han and Wahr*, 1995]. The GRACE gravity and GLAS altimeter data may also provide constraints on the historical ice evolution and mantle viscosity profile.

[6] Employing simulated GRACE gravity and GLAS altimetric data, a global inverse algorithm is developed that simultaneously solves for the present-day linear trends of ice mass change over Greenland and Antarctica and for global historical ice mass evolution. Present-day oceanic and hydrological mass rates over the rest of the global surface are also solved for in a geographically iterative sense. The discretized algorithm also incorporates realistic geographic boundaries. Our objective is to quantitatively assess the separability of current and past ice variations including the compaction factor, and spatiotemporal resolution and accuracy. Mantle viscosity profiles are fixed (not estimated) in each of our inverse simulations. We will, in certain cases, vary the lower mantle viscosity value to assess the effects of its uncertainty on the determination of ice mass variations. Also presented are the covariance analysis results when both ice mass variation and lower mantle viscosity are solved for together.

2. Gravity and Uplift Due to a Surface Mass Load

2.1. Forward Model

[7] Satellite gravity observations such as those by GRACE are commonly expressed in terms of spherical harmonic coefficients of the geoid (mean sea level equipotential surface) height above the reference ellipsoid, which is proportional to the perturbation of the gravitational potential [e.g., *Lambeck*, 1988]. The gravity and uplift responses of the Earth at present time t_p caused by past and present-day surface loading have typically been described in terms of load Love numbers and viscoelastic relaxation modes [e.g., *Mitrovica and Peltier*, 1989; *Han and Wahr*, 1995; *Vermeersen and Sabadini*, 1997], using a generic variable, such as

$$R = \frac{a}{M_e}\sum_{l=0}^{\infty}\sum_{m=-l}^{l}\frac{4\pi a^2}{2l+1}\int_{-\infty}^{t_p} L_{lm}(t) \cdot\left[R_l^E\delta(t_p-t)+\sum_{k=1}^{K}R_l^k e^{-s_l^k(t_p-t)}\right]dt Y_{lm}(\theta,\phi). \quad (1)$$

In equation (1), a and M_e are the radius and mass of the Earth, respectively. $L(\theta, \phi, t) = \Sigma_{l=0}^{\infty}\Sigma_{m=-l}^{l} L_{lm}(t)\ Y_{lm}(\theta, \phi)$ represents the harmonic expansion of the surface density of the load mass including the meltwater distributed in the oceans. Y_{lm} are the fully normalized spherical harmonic functions. R_l^E are the lth degree coefficients of the direct and elastic effect ($R_l^E = 1 + k_l^E$ for geoid, $R_l^E = h_l^E$ for uplift, k_l^E and and h_l^E are the usual elastic load Love numbers), δ is the Dirac delta function, and R_l^k and s_l^k are the amplitude and inverse decay time of the kth relaxation mode.

[8] The secular geoid rate due to the direct effect of present-day load variation plus elastic response can be derived from equation (1) by dropping the sum over k and taking the time derivative [see also, e.g., *Chao et al.*, 1987; *Dickey et al.*, 1997; *James and Ivins*, 1998; *Wahr et al.*, 1998]:

$$\dot{N}^{\mathrm{CUR}} = \sum_{l=0}^{\infty}\sum_{m=-l}^{l}\dot{N}_{lm}^{\mathrm{CUR}}Y_{lm}(\theta,\phi) = \sum_{l=0}^{\infty}\sum_{m=-l}^{l}\frac{a}{M_e}\frac{4\pi a^2}{2l+1}(1+k_l^E)\dot{L}_{lm}^{\mathrm{CUR}}Y_{lm}(\theta,\phi), \quad (2)$$

where $\dot{L}_{lm}^{\mathrm{CUR}}$ is the time rate of present-day surface density change. Equation (2) shows that the geoid harmonic rate $\dot{N}_{lm}^{\mathrm{CUR}}$ and the $\dot{L}_{lm}^{\mathrm{CUR}}$ have a one-to-one correspondence. k_l^E and h_l^E depend on the elastic structure of the Earth and are computed using the PREM Earth model. For R_l^k, and s_l^k, we use a reference viscoelastic Earth model consisting of an elastic lithosphere with 120 km thickness, an upper mantle extending to a 670 km depth with a viscosity of 1.0×10^{21} Pa s, a lower mantle with viscosity assumed to be 1.0×10^{22} Pa s, and an inviscid fluid core [*Han and Wahr*, 1995].

2.2. Reference Load Parameterization and Synthetic Data

[9] To study possible signatures and to perform inverse simulations, we first assume a loosely constrained global reference load variation scenario. Both simulated GRACE geoid and altimeter elevation rates are then generated from the reference scenario together with the anticipated dominant noise. These data sets are used in our linear discrete inverse algorithm to recover regional and global surface mass variations. The Greenland and Antarctic ice sheets are divided into

654 $2^\circ \times 6^\circ$ latitude/longitude grids. The various late Pleistocene ice sheets that completely disappeared 5–7 kyr ago are also divided into geographic grids with approximately 200 km spatial scale. The ocean and land areas not covered by the present or ancient ice are, however, described by $2^\circ \times 2^\circ$ grids for convenience in harmonic expansion.

[10] The linear rate of present-day ice mass change over Greenland is derived from a filtered version of *Huybrechts*' [1994] dynamic ice model prediction. For Antarctica, an imbalance scenario of *James and Ivins* [1997] [see also *Jacobs et al.*, 1992] is used. A saw-tooth version of ICE-3G model is used for the last glaciation-deglaciation cycle. We choose the time origin to be at the Last Glacial Maximum (LGM) 18 kyr before present (B.P.), so the present time is t_p = 18 kyr. The ice grows linearly from an initial time $t = -90$ kyr until the LGM at $t = 0$, then thins linearly until $t_0 = 14$ kyr. For the current continental ice sheets, a linear past trend twice that of the current rate is also assumed starting at $t_0 = 14$ kyr (4 kyr B.P.), and ending at $t_1 = 17.7$ kyr (0.3 kyr B.P.). The present-day secular rate, initiated at 0.3 kyr B.P., continues up to the present time t_p. The choice of the initiation epoch for the present-day trend is to have a negligible viscoelastic effect on modern geodetic data but is otherwise arbitrary. For both historical and present-day ice mass variations, corresponding meltwater is distributed eustatically over the current oceans. While the eustatic approximation serves our present purpose, a more accurate sea level theory should be used to model the real data [e.g., *Tamisiea et al.*, 2001].

[11] The present-day spherical harmonic rates of oceanic mass change (independent of meltwater) are based on a variant of the Parallel Ocean Program general circulation model developed at Los Alamos National Laboratory [*Dukowicz and Smith*, 1994; M. Molenaar and F. Bryan, personal communication, 1998], while the present-day hydrological mass rates are constructed from a combination of a land-surface water and energy-balance model and a high-resolution climate model at the Geophysical Fluid Dynamics Laboratory in Princeton (C. Milly and K. Dunne, personal communication, 1999). A mask function has been projected onto the hydrological model output to remove the hydrological mass rates from continental ice areas where they are indistinguishable from the ice mass variations. Both models are adapted to conserve mass by distributing the excess mass uniformly over the oceans or land. We assume that the periods of oceanic and hydrological variations are relatively short compared to the viscoelastic relaxation times, so that any small historical variations arising in these models are disregarded. Only the deglaciation-induced meltwater distribution in the oceans is retained in the inverse algorithm.

[12] Our choice of a universal saw-tooth function is certainly an oversimplification and more realistic global time functions can be used in future studies. Although a small deviation from the true time function should not significantly alter our error estimates, gravity observations may be more sensitive to deglaciation events occurring more recently than 18 kyr B.P., such as those in Antarctica and/or Greenland. The ice models could all have considerable uncertainties. Our assumption that the recent past rate is twice the present-day trend is arbitrary, serving only as an illustrative proxy model in order to examine the potential information content implied by the combined satellite data, model parameterization and formal inversion. However, since the inversion for LGM height and ice mass rates at present and in the past is linear, partial derivatives of the data with respect to these parameters do not depend on their values assumed in the model. On the other hand, partial derivatives with respect to the time parameters depend on the magnitude of the load. The inverse sensitivity to these parameters should be interpreted with caution, as there are possible unmodeled errors in the reference load scenario.

[13] The ice mass within each grid is then approximated by a circular disc with the same area as the grid, so the Legendre polynomial expansion derived by *Farrell* [1972] is applicable. The secular rate of geoid coefficients $\dot{N}_{lm}$ up to degree and order 90 for the reference load are computed from the time derivative of equation (1). The summation for the instantaneous elastic uplift is carried out to degree 512 for each grid [*James and Ivins*, 1998]. The viscous uplift computation, however, is only carried out to degree 90 since higher degree terms are filtered out by the elastic lithosphere in the reference Earth model.

3. Grid Inverse Simulation

3.1. Global and Regional Inverse Problems

[14] Inversion of secular satellite gravity data alone for global present-day and historical surface mass variations is an underdetermined problem. Over Greenland and Antarctic ice sheets, the addition of ice altimetry will help only to the extent that the compaction error described in the introduction is smaller or smoother than the present-day ice mass variations. Another source of underdeterminedness is the present-day hydrological changes over land that was once covered by the ancient ice sheets. In addition, there may be a trade-off between mantle viscosity and historical load mass variations in interpreting modern geodetic data [*Mitrovica et al.*, 1993; *Lambert et al.*, 2001]. Since present-day and historical ice mass variations are of primary interest, we first solve for ice load parameters with fixed Earth models, and treat such compaction, deglaciated area hydrology and mantle viscosity mismodeling signatures as additional noise in the data, rather than as estimated parameters. We begin with a baseline inverse solution, using only instrument noise in the data. This can be compared with inverse results using data with various additional noise to assess the level of contamination on the other parameter solutions. Finally, we conduct covariance analyses to investigate if the underdeterminedness or ambiguities can be substantiated or if more information can be derived from the data by estimating additional parameters.

[15] Our baseline inversion solves for global secular surface mass variations. These include present-day oceanic and hydrological mass variations over oceanic and land (not covered by ancient or current ice) grids, respectively. Two parameters are solved for over each ancient ice grid: the LGM ice height and the linear deglaciation time. For each current ice grid, in addition to the main-phase deglaciation parameters, we also solve for a present-day secular ice mass rate and a trend for the recent past (up to 0.3 kyr B.P.; hereinafter termed the ''recent past trend''). Also, one correction to the starting time, t_0, of the recent past trend Δt_0, is solved for over each continental ice sheet. Since meltwater is a dependent variable, it is not estimated explicitly. Mass conservation is enforced using a fictitious zero degree geoid observable with a very small uncertainty.

[16] After grid parameterization and linearization, the observation equation for our global inverse problem can be generally written as

$$\mathbf{L} = \mathbf{AX} + \mathbf{BY} + \mathbf{\Delta}. \quad (3)$$

L is the 8942-dimension data vector including geoid height rate up to degree/order 90 and one mean altimetric elevation rate over each current ice grid. **X** is the 3413-dimension parameter vector describing present-day and past surface mass changes over the current or ancient ice sheets as described above. **Y** is the 9458-dimension parameter vector for present-day surface mass variation over the vast areas of the oceans and land not covered by current or ancient ice. $\mathbf{\Delta}$ represents the sum of measurement noise and the unmodeled signal in the data such as those mentioned above.

[17] We assume the a priori mean to be zero for all linearized parameters. The corresponding a priori covariance matrix is taken to be diagonal with very large variances so that no significant amplitude constraints are placed on the model parameters except as otherwise noted. A diagonal measurement covariance matrix is also used in this study. The secular geoid coefficient uncertainties are derived from semianalytical prediction including major error sources anticipated for the GRACE mission (GRACE Project Science and Mission Requirements Document). Since errors in atmospheric mass variation models have an insignificant secular component [*Wahr et al.*, 2000; *Velicogna et al.*, 2001], they are not included in our study. The GLAS elevation uncertainty will be 1 cm, or less, for the minimum grid box of 10 km × 10 km and each 6-month repeat track. This translates to a 1.5 mm/yr uncertainty in elevation rate observations over 5 years and the larger (∼200 km) current continental ice grid.

[18] In our regional analysis experiments, we assume that there is no secular surface mass variation over the oceans and land areas not covered by ancient or current ice sheets other than the meltwater, or equivalently, $\mathbf{Y} = \mathbf{0}$. Hence only parameters over the current and ancient ice grids (**X**) and the associated posterior covariance matrix are estimated using the standard least squares procedure from GRACE secular geoid data and covariances. Here, mass conservation is assured by explicitly tracking the meltwater transfer in the model.

3.2. Inverse Strategy

[19] The global inversion is computationally challenging due to the vast area occupied by the oceans and hydrological land with active mass variations ($\mathbf{Y} \neq \mathbf{0}$). A simplified treatment is used in our study. Since the spherical harmonic coefficient of the present-day surface mass change $\dot{L}_{lm}^{\mathrm{CUR}}$ and the coefficient of the resulting geoid change $\dot{N}_{lm}^{\mathrm{CUR}}$ have a simple relation (equation (2)), one can easily obtain the surface mass variation without matrix inversion if the geoid height rate is known and if the viscoelastic signal in the solid Earth is ignored. This fact is exploited in our study to avoid the very large (12,871 dimension) normal matrix. To obtain a first approximation for **Y**, the rates of geoid coefficients contained in **L** are converted into rates of global surface mass harmonic coefficients. Gaussian averages of the surface mass changes are then derived over each 2° × 2° grid by multiplying the coefficients with degree-dependent smoothing factors and summing the harmonic terms over degree and order [*Jekeli*, 1981]. A Gaussian half scale (see below) of 50 km is used for the averages. The estimate $\hat{\mathbf{Y}}$ is then obtained by multiplying the global surface mass distribution by a mask function that is unity over oceans and land away from the ice sheets but zero over the current and ancient ice grids. The first approximate solution for **X** results from the new observation equation $\mathbf{L} - \hat{\mathbf{Y}} = \mathbf{AX}$ using the standard least squares method. The next iteration repeats the above procedure except that $\mathbf{L} - \mathbf{A}\hat{\mathbf{X}}$ is used in place of **L** to derive a new $\hat{\mathbf{Y}}$, thus also providing a new estimate of **X**. The residuals and the solutions for both **X** and **Y** converge after more than 100 iterations.

[20] The inverted parameters over each ice grid have large errors due to the error structure in the satellite gravity measurements. Instead of using the box-car averages, we perform a running average procedure with a Gaussian kernel at each grid *i*:

$$\bar{X}_i = \sum_{j=1}^{n} A_j e^{-\ln 2(s_{ij}/s_0)^2} \hat{X}_j \Big/ \sum_{j=1}^{n} A_j e^{-\ln 2(s_{ij}/s_0)^2}, \quad (4)$$

where $\hat{X}_j$ is the least squares estimate for the parameter of the *j*th grid, *n* is the total number of grids, A_j is the area of the *j*th grid, s_{ij} is the distance between the *i*th and *j*th grid centers, and s_0 is the Gaussian half scale. Note that such an averaging kernel is also unimodular, meaning that the sum of the averaging coefficients is unity. The average centered at each grid is used to represent the grid value and hereinafter defines the s_0 Gaussian average. The s_0 is a measure of spatial resolution and is chosen to reach a reasonable balance with the uncertainty level of the corresponding Gaussian averages. The RMS and mean values of the running Gaussian averages summarize the inverse results over certain geographic areas. The covariance of the Gaussian averaged parameters are derived from the posterior covariance matrix for the original parameters according to the law of error propagation [*Rao*, 1973]. The inverse recovery error is obtained from the difference between the Gaussian averages of the reference and inverted parameter values.

[21] For regional analysis, the resulting posterior covariance can be used to assess separability, accuracy and resolution. This will be supported by the inverted result when it is compared with the reference parameter state used in the simulation. The iterative global solution, however, does not yield any meaningful posterior covariance. Separability, resolution, and accuracy can only be inferred by comparing the inverted result with the reference parameter values, both Gaussian averaged with a consistent spatial scale. It should be noted here that the recovery errors in the simulated inverse study are not exactly the same as formal uncertainties in the estimates, which can be considerably larger or smaller. Instead, they are just one realization of the random vector with the formal uncertainties as its standard deviations. Simultaneous global grid solutions would provide a more robust information content and an effort is underway to achieve such solutions using massively parallel computing architectures [*Wang and Wu*, 2002].

4. Results and Discussion

4.1. Regional Recovery Using Gravity Data

[22] Our regional analysis shows that by isolating secular surface mass variations geographically and using a fixed

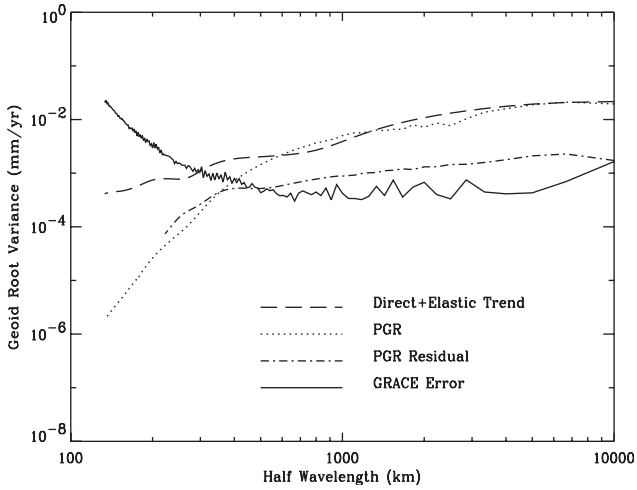

Figure 1. Square root of the geoid degree variance due to the gravitational and elastic effects of the current Greenland linear trend; total viscous response to late Pleistocene deglaciation and the recent past trend (PGR); residual total viscous response from the regional inversion; and the GRACE geoid error.

Earth rheological structure, the synthetic GRACE global gravity data alone can separate the present-day and historical ice mass variations. As an example, both present-day and past ice mass variations over Greenland are estimated along with late Pleistocene Laurentian deglaciation using simulated GRACE geoid coefficients. Most of the significant features in the present-day ice mass imbalance model are recovered by the inversion. The RMS formal uncertainty for the 250-km Gaussian average present-day rates in equivalent ice thickness is 2.1 cm/yr. The uncertainty for the mean thickness change of the ice sheet is 3 mm/yr, corresponding to 0.01 mm/yr in sea level rise due to Greenland contribution.

[23] The geoid root variances of different signatures are shown in Figure 1. Examination of the spatial wavelength spectrum reveals that the viscoelastic Earth behaves like a low-pass filter so that the power of the viscous response to load variation diminishes toward the shorter wavelengths (also see the map view figures of *Ivins et al.* [2001]). In the parameterization both historical and current load mass variations are allowed the same spatial scale by using the same grids, but the responses are obviously different in spatial pattern, indicating that the columns of the measurement matrix **A** are linearly independent. This allows the high-resolution global GRACE gravity measurements to distinguish between them [also see *Kaufmann*, 2000].

[24] However, the Earth's dynamic ocean and hydrological land areas are known to undergo interdecadal and intradecadal variability, and these processes may involve significant mass variations. As pointed out by *Wahr et al.* [2000], we face the difficulty of working with data having a time span that is short in comparison to the long-period variations that are of interest. Also, the regional grid algorithm is sensitive to unmodeled signals in the data from the omitted geographic regions. Although providing substantial insight, the regional algorithm has limited applicability to future gravity mission data. In particular, oceanic and hydrological mass variations must be included in the global inverse solution.

4.2. Global Inverse: Recovery Over Greenland and Antarctica

[25] Over the current continental ice sheets, if the surface density profile remains constant, the combination of GRACE geoid and ice altimetry in the global solution effectively separates the present-day ice mass variation signatures and viscous PGR signatures in both data types. This is shown in our baseline inverse result. The RMS and mean 250-km Gaussian average bedrock viscous uplift recovery errors are listed in Table 1, using GLAS instrument noise σ_h = 1.5 mm/yr over each grid. The significant reduction of the systematic viscous uplift error from the order of centimeters per year to that of millimeters per year highlights the potential contribution of the combined GLAS altimetry and GRACE gravity data sets to the determination of present-day ice mass imbalance. The mean ice mass imbalance recovery errors over Greenland and Antarctica are −0.5 and 0.3 mm/yr, respectively, consistent with errors due to GLAS noise only.

[26] This result is in agreement with that of *Wahr et al.* [2000], who used an iterative approach in applying ice topography and gravity data guided by approximate observation equations in the spherical harmonic domain. The spherical harmonic rates for the geoid and the ice topography can be written, respectively, as

$$\dot{N}_{lm} = \frac{4\pi a^3}{M_e}\frac{1+k_l^E}{2l+1}\dot{L}_{lm}^{\mathrm{CUR}} + \dot{N}_{lm}^{\mathrm{PGR}}, \tag{5}$$

$$\dot{U}_{lm} \approx \left(\frac{1}{\rho_{\mathrm{ice}}} + \frac{4\pi a^3}{M_e}\frac{h_l^E}{2l+1}\right)\dot{L}_{lm}^{\mathrm{CUR}} + \left(\frac{2l+1}{2}\right)\dot{N}_{lm}^{\mathrm{PGR}} + C_{lm}. \tag{6}$$

Here ρ_{ice} is the density of solid ice. The 2nd term in the topography change equation is the PGR uplift coefficient $\dot{U}_{lm}^{\mathrm{PGR}} \approx [(2l+1)/2]\,\dot{N}_{lm}^{\mathrm{PGR}}$ [see *Wahr et al.*, 1995]. C_{lm} is the harmonic coefficient of the compaction error, which is zero for the baseline case. Although gravity and altimetric techniques are both affected by the ambiguity between the current and past load variation, they measure entirely

Table 1. Recovery Error Over Current Continental Ice Sheets[a]

	σ_h = 1.5 mm/yr	σ_h = 7 mm/yr	Δh = 5 mm/yr	$\Delta\nu_{\mathrm{LM}}$ = -5.5×10^{21} Pa s σ_h = 1.5 mm/yr	Unit
GRE RMS u_{PGR}	0.2	1.0	1.3	0.2	mm/yr
GRE mean u_{PGR}	0.04	0.02	−1.3	0.02	mm/yr
ANT RMS u_{PGR}	0.3	0.5	1.2	0.2	mm/yr
ANT mean u_{PGR}	−0.2	−0.1	−1.2	−0.1	mm/yr
GRE RMS h_{LGM}	36	96	275	80	m
GRE mean h_{LGM}	−2	18	−273	−19	m
ANT RMS h_{LGM}	16	48	292	52	m
ANT mean h_{LGM}	−1	2.3	−291	7	m
GRE RMS $\dot{h}_{\mathrm{past}}$	0.3	0.9	2.6	5.1	cm/yr
GRE mean $\dot{h}_{\mathrm{past}}$	0.04	0.1	2.6	−5.1	cm/yr
ANT RMS $\dot{h}_{\mathrm{past}}$	0.2	0.7	2.5	0.8	cm/yr
ANT mean $\dot{h}_{\mathrm{past}}$	−0.02	−0.3	2.5	−0.7	cm/yr

[a] The PGR uplift (u_{PGR}) errors are represented by 250-km Gaussian averages, while the LGM height (h_{LGM}) and past rate ($\dot{h}_{\mathrm{past}}$) errors are represented by 450-km Gaussian averages. $\Delta\nu_{\mathrm{LM}}$ is the fixed bias in the lower mantle viscosity. GRE, Greenland; ANT, Antarctica.

different physical quantities not proportionally affected by historical and current ice mass changes. In a schematic way, there are two different observables in the harmonic domain: geoid and uplift, and two unknowns (with $C_{lm} = 0$): secular present-day ice mass change and PGR geoid rate. Our method is different from that of *Wahr et al.* [2000] in that the approximate linear proportionality between PGR uplift and gravity is not employed, and our explicit parameters for the PGR are historical load mass variations. However, equations (5) and (6) provide a good physical explanation of why the gravity/altimetry data sets can resolve present-day secular ice mass change and PGR geoid or PGR uplift signatures.

[27] Moreover, the combination of GRACE gravity data with ice altimetry offers a window through which we might be able to view the history of evolution of the continental ice sheets. For example, with a fixed mantle viscosity profile and assuming well-known deglaciation time intervals with no linear trend in the recent past from t_0 to t_1, then the combination of data can be used to determine the LGM height of these ice sheets. Figure 2 shows the 450-km Gaussian average recovery errors in Antarctica using the σ_h = 1.5 mm/yr altimeter noise. The RMS and mean recovery errors are also listed in Table 1 (rows 5 to 8). On the other hand, if the late Pleistocene deglaciation events are well constrained, the gravity and altimetry data can be used to infer a recent past trend separately from the present-day trend. The trend starting from 4 kyr B.P. can be determined quite well. The RMS and mean 450-km Gaussian average recovery errors in the recent past trend are also listed in Table 1 (rows 9 through 12).

[28] However, the contemporary geodetic data sets lack any substantive temporal resolution. This is to be expected since 5 years of observation is, in effect, a snap shot in time, when compared with glaciation and deglaciation timescales. Our simulations show that the ancient deglaciation and a recent past trend cannot be meaningfully separated using the gravity/altimetry data sets alone. Without any a priori information constraining the late Pleistocene deglaciation, the geodetic data sets cannot even separate the LGM height and the deglaciation time over the grids. If these are solved for together, the RMS 450-km Gaussian average recovery error for the LGM height over the current ice sheets becomes 1.1 km. The mean recovery errors on the other hand are smaller, 296 m for Greenland and 61 m for Antarctica.

[29] We now turn to the effects of the compaction errors inherent in converting the altimeter elevation data to the ice mass variation. *Wahr et al.* [2000] have estimated that the temporal RMS 5-year spatial mean compaction error could be 4.5 mm/yr in equivalent water thickness, and the mean compaction error over a 5-year period can be as large as 18 mm/yr. The compaction errors also have considerable spatial variability with an anticipated correlation length of 1000 km [*Arthern and Wingham*, 1998]. For Antarctica, the average RMS compaction error about the spatial mean values over 170 years is estimated to be 6.8 mm/yr. In this paper we use a constant 5 mm/yr bias and a 6.8 mm/yr random grid error as additional noise in altimeter elevation rate measurements to simulate the possible mean and spatially variable compaction errors.

[30] When the random instrument and compaction noise σ_h = 7 mm/yr is used in the altimeter data, the RMS 250-km

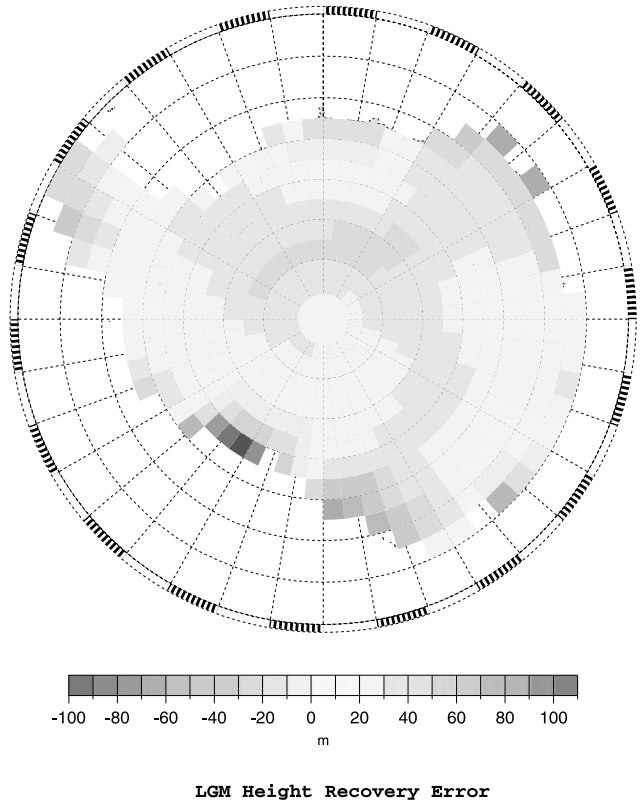

Figure 2. The 450-km Gaussian average inverse recovery errors in the LGM heights over Antarctica. Elevation rate noise is assumed to be 1.5 mm/yr over each grid for 5 years of GLAS altimeter measurements. See color version of this figure at back of this issue.

Gaussian average total viscous uplift error becomes larger. However, the mean viscous uplift errors for both Greenland and Antarctica remain small (see column 2 in Table 1). The mean present-day ice mass imbalance recovery errors for Greenland and Antarctica are −0.5 and −0.1 mm/yr, respectively, in equivalent ice thickness. Recovery errors for either the LGM ice heights or the recent past trends also increase modestly (Table 1 and Figure 3). In contrast, the bias Δh = 5 mm/yr in the altimeter elevation rate measurement across Greenland or Antarctica (in addition to the instrument noise) causes both RMS and mean viscous uplift errors to increase significantly. The mean Greenland mass imbalance error becomes 6.3 mm/yr in equivalent ice thickness. The root cause of this increase is, essentially, the accretionary effects of the compaction and PGR errors, $\Delta h - \mu_{PGR}$ (see Table 1). The bias also strongly contaminates the LGM height and the recent past trend estimates. In section 4.5 we discuss methods for reducing the compaction error through estimation.

4.3. Global Inverse: Recovery over Ancient Ice Sheets

[31] The recovery errors of the 450-km Gaussian average LGM equivalent ice height over the ancient Laurentian ice sheet are plotted in Figure 4. The errors tend to increase toward the boundary of each large ice sheet. Errors are also larger for smaller ice sheets since satellite gravity data poorly resolve them. The RMS and mean 450-km Gaussian

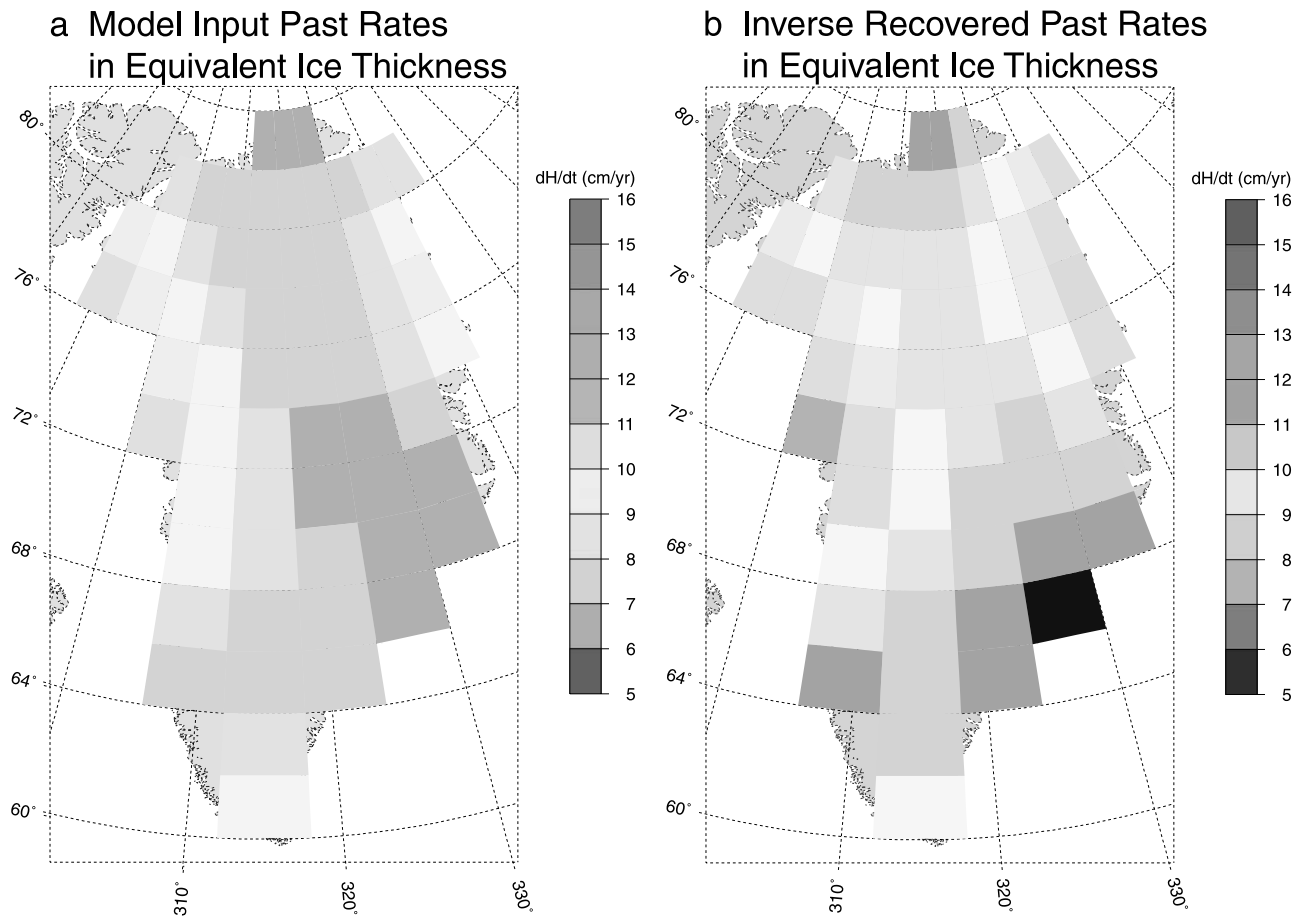

Figure 3. (a) Simulation input model and (b) inverse recovered past trends in Greenland. Both are 450-km Gaussian averaged; 7 mm/yr altimeter elevation rate noise is assumed to reflect instrument and possible spatially variable compaction errors. See color version of this figure at back of this issue.

average recovery errors are listed in Table 2 for two cases of inverse simulations. In the first case, the deglaciation time is fixed and no hydrological signatures from the area covered by the ancient ice sheets are included in the simulated data. When the hydrological signatures from the area are included as noise in the simulated data and deglaciation times with a priori uncertainty of 5 kyr for each grid are also estimated in the second case, the RMS recovery error becomes 2–3 times larger. The mean recovery error, however, is not significantly perturbed. The dominant source for the RMS errors in this case is the hydrological contamination of the gravity data.

4.4. Effects of Uncertainty in Lower Mantle Viscosity

[32] Currently, the range of lower mantle viscosity estimates spans more than one order of magnitude. To examine the effects of this uncertainty, we use the fixed reference viscoelastic Earth model to generate the simulated data but carry out inverse analyses assuming a different value of lower mantle viscosity. This is equivalent to introducing mismodeling errors in the data due to a bias in this parameter, $\Delta\nu_{\mathrm{LM}}$. Our ability to recover the present-day ice mass variation, elastic uplift, and PGR uplift does not depend on the knowledge of the lower mantle viscosity value (Table 1). This result is consistent with the analysis of *Wahr et al.* [2000]. The knowledge of viscosity profile, however, is crucial to the determination of historical ice evolution. For example, when a bias $\Delta\nu_{\mathrm{LM}} = -5.5 \times 10^{21}$ Pa s is introduced in the Earth model, the recovery errors in the recent past trends and LGM ice heights become considerably larger using 1.5 mm/yr altimeter noise and without compaction error (Table 1) or hydrological contamination (Table 2).

4.5. Constraints on Mean Compaction and Lower Mantle Viscosity

[33] As discussed above, the average compaction error across each continental ice sheet is the dominant factor in degrading the solution approach for determining both the present-day ice mass imbalance and for constraining historical ice load evolution. Knowledge of the mantle viscosity profile is also critical to unraveling the ice load history. Whether a mean compaction error per ice sheet, or a uniform lower mantle viscosity value, can be solved simultaneously along with the ice mass variation from the satellite altimeter and gravity data then becomes an intriguing question. Normally, our geographically iterative algorithm cannot compute a posterior covariance matrix, as already mentioned. However, we can conduct covariance analyses based on different simulated inversions to derive the formal uncertainty for these two parameters if either one were estimated together with the surface mass parameters.

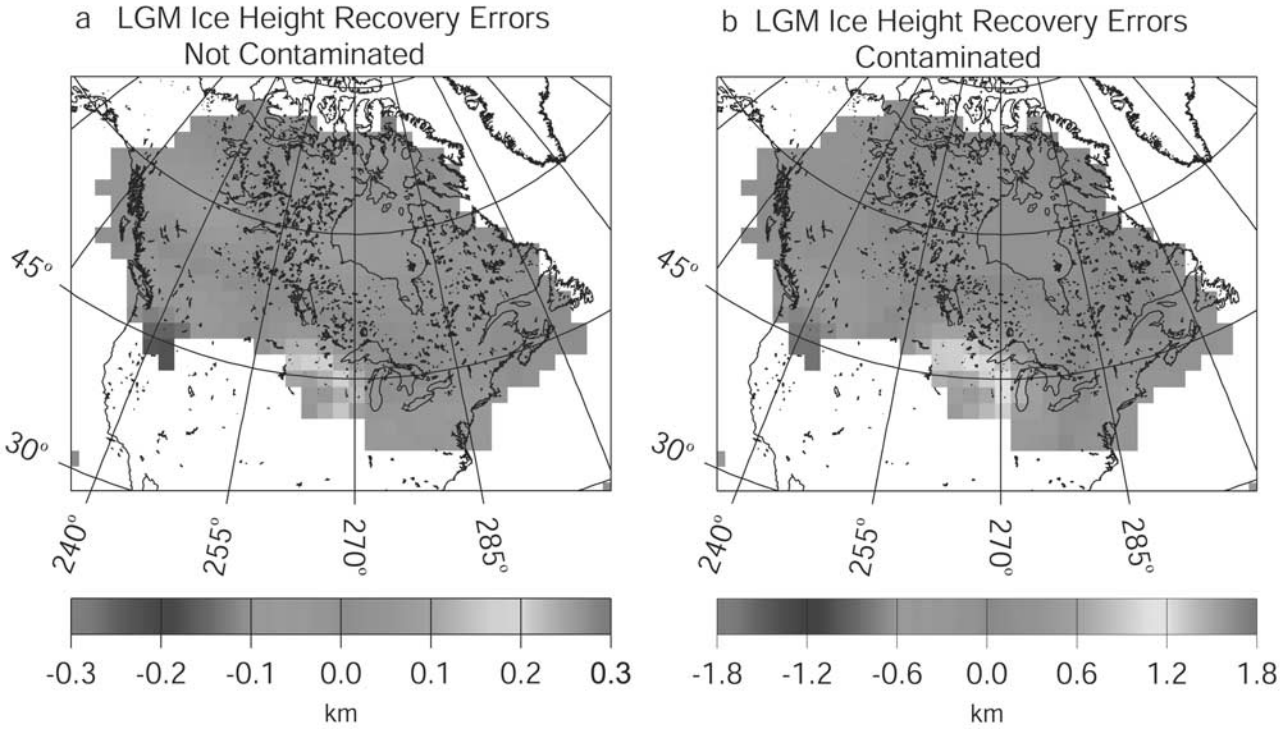

Figure 4. The 450-km Gaussian average inverse recovery errors in the LGM ice heights over the ancient Laurentian ice sheet. (a) Simulated data that do not include hydrological noise from the area once covered by the ice sheet and deglaciation times are assumed known and (b) data that include hydrological noise from the area and deglaciation times are also solved for with a priori uncertainty of 5 kyr for each grid. See color version of this figure at back of this issue.

[34] For our baseline inversion, only instrument noise $\mathbf{\Delta} = \mathbf{\Delta_0}$ is included. Equation (3) can be rewritten in the following form:

$$\mathbf{L_0} = \mathbf{FZ} + \mathbf{\Delta_0}, \tag{7}$$

where $\mathbf{F} = [\mathbf{A}\ \mathbf{B}]$ and $\mathbf{Z^T} = [\mathbf{X^T Y^T}]$ is the transpose of $\mathbf{Z}$. The residual vector is then

$$\mathbf{V} = \left[\mathbf{I} - \mathbf{F}(\mathbf{F^T P F})^{-1}\mathbf{F^T P}\right]\Delta_0 = \mathbf{C}\Delta_0, \tag{8}$$

where $\mathbf{I}$ is the identity matrix and $\mathbf{P}$ is the inverse of the data noise covariance matrix. The χ-square of the residuals is

$$\mathbf{V^T P V} = \Delta^{\mathbf{T}}\mathbf{C^T P C}\Delta_0. \tag{9}$$

In the second inversion, the noise also includes a mismodeling error, $\mathbf{\Delta} = \mathbf{\Delta_0} + \mathbf{G}b$, where b is either a constant compaction error or an error in the lower mantle viscosity value. $\mathbf{G}$ is a column matrix containing corresponding partial derivatives. The new vector observation equation becomes:

$$\mathbf{L} = \mathbf{FZ} + \mathbf{G}b + \Delta_0. \tag{10}$$

We carry the iterative least squares solution solving only for $\mathbf{Z}$. The residual and χ-square in this case are

$$\mathbf{V_b} = \mathbf{C}(\mathbf{G}b + \mathbf{\Delta}_0), \tag{11}$$

$$\mathbf{V_b^T P V_b} = \mathbf{G^T C^T P C G}b^2 + \mathbf{V^T P V} + 2b\mathbf{G^T P V}. \tag{12}$$

All terms in equation (12) are known except the first term on the right because the matrix $\mathbf{C}$ is not computed by the iterative least squares inversion.

[35] If we solve $\mathbf{Z}$ and b together, the posterior covariance matrix of the solution would be

$$\mathbf{D} = \begin{pmatrix} \mathbf{D_{11}} & \mathbf{D_{12}} \\ \mathbf{D_{21}} & \mathbf{D_{22}} \end{pmatrix} = \mathbf{N}^{-1} = \begin{pmatrix} \mathbf{N_{11}} & \mathbf{N_{12}} \\ \mathbf{N_{21}} & \mathbf{N_{22}} \end{pmatrix}^{-1} = \begin{pmatrix} \mathbf{F^T P F} & \mathbf{F^T P G} \\ \mathbf{G^T P F} & \mathbf{G^T P G} \end{pmatrix}^{-1}, \tag{13}$$

where $\mathbf{N}$ is the normal matrix of the least squares problem. $\mathbf{D_{22}}$ is the scalar posterior covariance of b. By a matrix version of Gaussian reduction, it can be demonstrated that

$$\mathbf{D_{22}} = (\mathbf{N_{22}} - \mathbf{N_{21}}\mathbf{N_{11}^{-1}}\mathbf{N_{12}})^{-1}. \tag{14}$$

Table 2. Recovery Error in Ancient Ice LGM Heights[a]

	Laurentide		All Ancient Ice	
	RMS	Mean	RMS	Mean
$\dot{h}_{\text{hydro}} = 0$, $\sigma_{t_0} = 0$	93	−61	130	−95
$\dot{h}_{\text{hydro}} \neq 0$, $\sigma_{t_0} = 5$ kyr	270	−24	280	86
$\Delta\nu_{\text{LM}} = -5.5 \times 10^{21}$ Pa s	362	354	303	259

[a] Units are meters. The $\dot{h}_{\text{hydro}}$ is the present-day rate in equivalent water thickness due to hydrological variations. The signal from the model is included in the data ($\dot{h}_{\text{hydro}} \neq 0$) but is not solved for. It is not included in the data ($\dot{h}_{\text{hydro}} = 0$). σ_{t_0} is the a priori uncertainty for the deglaciation time over each grid; $\sigma_{t_0} = 0$ means that the deglaciation time is fixed. $\Delta\nu_{\text{LM}}$ is the fixed bias in the lower mantle viscosity.

Since $\mathbf{D_{22}}$ is a scalar, we therefore have the formal uncertainty of b as

$$\sigma_b = \sqrt{\mathbf{D_{22}}} = 1/\sqrt{\mathbf{G^T C^T P C G}}. \quad (15)$$

The denominator can be derived from the known terms of equation (12) and the value of b.

[36] For the mean Antarctic compaction factor, the posterior formal uncertainty is computed to be 1.5 mm/yr. This is the uncertainty if the mean compaction were estimated simultaneously with the global surface mass variation $\mathbf{Z}$, using 1.5 mm/yr instrument noise as the grid uncertainty in elevation rate measurements. This formal uncertainty result is also supported by our iterative simulation when b is solved together with $\mathbf{Z}$. The recovery error for b is 2 mm/yr. This result also does not depend on accurate knowledge of the lower mantle viscosity value. When 7 mm/yr random grid error is used for the elevation rate measurements, the formal uncertainty for the mean compaction factor becomes 3.1 mm/yr. The formal uncertainty for the mean Greenland compaction is 2.7 mm/yr, using a 1.5 mm/yr instrument noise.

[37] In principle, the high-resolution altimeter and gravity data combination should be able to constrain the present-day ice mass variation, PGR uplift, and some spatial averages of the compaction errors simultaneously. This can be seen by examining equations (5) and (6) with $C_{lm} = F_{lm} b \neq 0$, where F_{lm} are known coefficients. The additional parameter b would at first seem to introduce an apparent rank deficiency in the equations. However, as can be seen in Figure 1, the PGR geoid variations have diminished power toward the high degrees. For physically plausible scenarios and a reasonably thick lithosphere, the high-degree PGR terms can be dropped from the equations, which then allow the mean compaction b to be resolved by the data combination, even though the adjusted bias b in the altimetric data does not directly affect the gravity. In practice, the magnitude of this potentially important constraint on b depends on such factors as the magnitude and geographic correlation of the compaction errors, as well as eventual measurement noise in both gravity and altimetric elevations. Future study of this issue using a simultaneous inversion procedure and geographically correlated compaction errors is desirable.

[38] The formal uncertainty of lower mantle viscosity is estimated to be 3×10^{22} Pa s if it is estimated together with the ice parameters. We should point out that rigorous inversion for the lower mantle viscosity has to deal with the issue of nonlinearity [*Mitrovica and Peltier*, 1993]. Our purpose here is to provide a rough estimate of the information content of the data with respect to this parameter. When the residuals are examined geographically for two inversion cases with the same simulated data but different fixed lower mantle viscosity values, they retain the same basic amplitudes and spatial patterns. Similar results are also obtained when the deglaciation times and recent past trends for the ice sheets are fixed and an inversion is only performed for LGM ice heights. This indicates that the satellite data alone cannot effectively separate the viscosity profile and ice load history.

5. Conclusions

[39] Secular gravity variations to be measured by the GRACE mission are integral constraints on the near-surface and deep mass transport in the dynamic Earth. Combined use of GRACE measurements with other geodetic or geological data sets have the potential to enhance the separation among geophysical sources and to improve the accuracy/resolution for surface mass variations and deformation. As an initial step, this paper has sought to evaluate the information content of the concurrent GRACE gravity and GLAS altimetry data in terms of current and past cryogenic, oceanic and hydrological surface mass variations within a discrete global inverse framework. Equivalent ice or water thickness changes are inverted from synthetic data and compared to the input parameters to assess recovery errors and resolution. Covariance analyses have addressed the sensitivities to critical parameters such as mean compaction errors over Greenland and Antarctica, and lower mantle viscosity. The main conclusions are as follows:

1. The gravity and altimetry data combination reduces the bedrock PGR uplift error for Greenland and Antarctica to the level of 1 mm/yr. Also, the mean compaction error can be constrained for large continental ice sheets. Our simulation and covariance analysis suggest a formal uncertainty of about 3 mm/yr for the mean compaction error in Antarctica. Compared with "altimeter only" solutions, the data combination has the potential to reduce systematic PGR and compaction errors in the mean Antarctic present-day ice mass imbalance determination from 1–2 cm/yr to 4 mm/yr, corresponding to an error of 0.1 mm/yr in sea level contribution. The compaction error may have considerable large scale spatial variability over Greenland and Antarctica. GPS uplift measurements on exposed bedrock can provide valuable constraints on these errors, thus better constraining both present-day mass imbalance and PGR [*Velicogna and Wahr*, 2002].

2. The new data combination will also provide combinations of historical ice load variables that can be useful in unraveling the history of the ice sheet. However, to adequately resolve the loading history using the methods outlined here, an accurate knowledge of the mantle's viscosity profile is required a priori. The global secular gravity and ice altimetry data will not be able to resolve surface load history and lower mantle viscosity simultaneously. Combining the high spatial resolution geodetic data with the RSL records might provide a resolution of this difficulty.

3. For a fixed viscosity profile, the RMS 450-km Gaussian average LGM heights of ancient ice sheets can be constrained to about 300 m with reasonable additional constraints on the deglaciation time. A major source of error in this reconstruction is the unknown hydrological mass variation over the once ice-covered areas. The mean LGM ice height across each large ice sheet can, nonetheless, be constrained to levels well below 100 m by the secular geodetic data, despite the hydrological contamination. Any reduction in the hydrological contaminations from in situ data would lead to a better map of the equivalent ancient ice heights. The combination of satellite gravity with RSL and GPS monitoring should significantly improve the reconstruction of the ancient ice sheets and inferences of mantle viscosity profile [e.g., *Milne et al.*, 2001].

4. For the existing continental ice sheets, the contemporary altimeter/gravity data cannot discern, in and of

themselves, load variation events in the past, especially in regard to distinguishing between late Pleistocene deglaciation and load variations occurring over the last few thousand years. Provided that any recent past trends are independently constrained, the onset and deglaciation times should be better constrained by the RSL data, which have better time resolution than contemporary geodesy. Then the spatial distribution of LGM heights determined by the geodetic data shall be an invaluable complement to reconstructions of the ice sheet history. This may be especially true for the Antarctic ice sheet where local RSL records are sparse. The secular geodetic data can also be used to detect any ice mass trends in the last few thousand years if the late Pleistocene and early Holocene deglaciation are separately determined. Such separation of the historical load events over the current polar ice sheets will also benefit from more data such as ice core, dated volcanic ash and glacio-moraine deposits, and rock surface exposure ages [e.g., *Ackert et al.*, 1999; *Borns*, 2001; *Steig et al.*, 2001].

[40] **Acknowledgments.** This work was partially carried out at the Jet Propulsion Laboratory, California Institute of Technology, under contract with the National Aeronautics and Space Administration (NASA). Support by NASA's Polar and Solid Earth/Natural Hazard programs is acknowledged. We are grateful to Dazhong Han for his viscoelastic Green's functions, to Srinivas Bettadpur for discussions regarding GRACE error prediction, to Mery Molenaar and Frank Bryan for their oceanic estimates, and to Chris Milly and Krista Dunne for water storage data. We thank Donald Argus, Curt Davis, Bruce Haines, George Hajj, Philippe Huybrechts, Roberto Julio, Gerhard Kruizinga, Da Kuang, Jay Parker, Larry Romans, and Niels Reeh for help, discussion, or comments, Ab Davis and Byron Tapley for encouragement. Comments from Jerry Mitrovica, C. K. Shum, and an anonymous reviewer improved the manuscript.

References

Ackert, R. P., D. J. Barclay, H. W. Borns, P. E. Calkin, M. D. Kurz, J. L. Fastook, and E. J. Steig, Measurements of past ice sheet elevations in interior West Antarctica, *Science*, *286*, 276–280, 1999.

Arthern, R. J., and D. J. Wingham, The natural fluctuations of firn densification and their effect on the geodetic determination of ice sheet mass balance, *Clim. Change*, *40*, 605–624, 1998.

Borns, H. W., The glacial geological terrestrial record from west Antarctica with emphasis on the last glacial cycle, in *The West Antarctic Ice Sheet: Behavior and Environment*, *Antarctic Res. Ser.*, vol. 77, edited by R. B. Alley and R. A. Bindschadler, pp. 59–74, AGU, Washington, D. C., 2001.

Chao, B. F., W. P. O'Connor, A. T. C. Chang, D. K. Hall, and J. L. Foster, Snow load effects on the Earth's rotation and gravitational field, 1979–1985, *J. Geophys. Res.*, *92*, 9415–9422, 1987.

Davis, C. H., C. A. Kluever, and B. J. Haines, Elevation change of the southern Greenland ice sheet, *Science*, *279*, 2086–2088, 1998.

Dickey, J. O., et al., Satellite Gravity and the Geosphere: Contributions to the Study of the Solid Earth and Its Fluid Envelope, 112 pp., Natl. Acad. Press, Washington, D. C., 1997.

Dukowicz, J. K., and R. D. Smith, Implicit free-surface method for the Bryan-Cox-Semtner ocean model, *J. Geophys. Res.*, *99*, 7991–8014, 1994.

Farrell, W. E., Deformation of the Earth by surface loads, *Rev. Geophys.*, *10*, 761–797, 1972.

Han, D., and J. M. Wahr, The viscoelastic relaxation of a realistically stratified Earth, and a further analysis of postglacial rebound, *Geophys. J. Int.*, *120*, 287–311, 1995.

Huybrechts, P., The present evolution of the Greenland ice sheet: an assessment by modeling, *Global Planet. Change*, *9*, 39–51, 1994.

Ivins, E. R., X. Wu, C. A. Raymond, C. F. Yoder, and T. S. James, Temporal geoid of a rebounding Antarctica and potential measurement by the GRACE and GOCE satellites, in *I.A.G. Symposia 123: Gravity, Geoid and Geodynamics 2000*, edited by M. G. Sideris, pp. 361–366, Springer-Verlag, New York, 2001.

Jacobs, S. S., H. H. Hellmer, C. S. M. Doake, A. Jenkins, and R. M. Frolich, Melting of ice shelves and the mass balance of Antarctica, *J. Glaciol.*, *38*, 375–387, 1992.

James, T. S., and E. R. Ivins, Global geodetic signatures of the Antarctic ice sheet, *J. Geophys. Res.*, *102*, 605–633, 1997.

James, T. S., and E. R. Ivins, Predictions of Antarctic crustal motions driven by present-day ice sheet evolution and by isostatic memory of the Last Glacial Maximum, *J. Geophys. Res.*, *103*, 4993–5017, 1998.

Jekeli, C., Alternative methods to smooth the Earth's gravity field, *Rep. Dep. Geod. Sci. Surv. 327*, 48 pp., Ohio State Univ., Columbus, 1981.

Kaufmann, G., Ice-ocean mass balance during the late Pleistocene glacial cycles in view of CHAMP and GRACE satellite missions, *Geophys. J. Int.*, *143*, 142–156, 2000.

Krabill, W., R. Thomas, and S. Manizade, Greenland ice sheet thickness changes measured by laser altimetry, *Geophys. Res. Lett.*, *22*, 2341–2344, 1995.

Lambeck, K., *Geophysical Geodesy, The Slow Deformations of the Earth*, 718 pp., Oxford Univ. Press, New York, 1988.

Lambert, A., N. Courtier, G. S. Sasagawa, F. Klopping, D. Winester, T. S. James, and J. O. Liard, New constraints on Laurentide postglacial rebound from absolute gravity measurements, *Geophys. Res. Lett.*, *28*, 2109–2112, 2001.

Milne, G. A., J. L. Davis, J. X. Mitrovica, H.-G. Scherneck, J. M. Johansson, M. Vermeer, and H. Koivula, Space-geodetic constraints on glacial isostatic adjustment in Fennoscandia, *Science*, *291*, 2381–2385, 2001.

Mitrovica, J. X., and W. R. Peltier, Pleistocene deglaciation and the global gravity field, *J. Geophys. Res.*, *94*, 13,651–13,671, 1989.

Mitrovica, J. X., and W. R. Peltier, A complete formalism for the inversion of postglacial rebound data: Resolving power analysis, *Geophys. J. Int.*, *104*, 267–288, 1991a.

Mitrovica, J. X., and W. R. Peltier, Free air gravity-anomalies with glacial isostatic disequilibrium-load history effects on the inference of deep mantle viscosity, *Geophys. Res. Lett.*, *18*, 235–238, 1991b.

Mitrovica, J. X., and W. R. Peltier, Present-day secular variations in the zonal harmonics of Earth's geopotential, *J. Geophys. Res.*, *98*, 4509–4526, 1993.

Mitrovica, J. X., J. L. Davis, and I. I. shapiro, Constraining proposed combinations of ice history and earth rheology using VLBI determined base-line length rates in North America, *J. Geophys. Res. Lett.*, *20*, 2387–2390, 1993.

Nakada, M., and K. Lambeck, Glacial rebound and relative sea-level variations: A new appraisal, *Geophys. J. R. Astron. Soc.*, *90*, 171–224, 1987.

Nakada, M., and K. Lambeck, The melting history of the late Pleistocene Antarctic ice sheet, *Nature*, *333*, 36–40, 1988.

Peltier, W. R., and J. T. Andrews, Glacial-isostatic adjustment, I, The forward problem, *Geophys. J. R. Astron. Soc.*, *46*, 605–646, 1976.

Rao, C. R., *Linear Statistical Inference and Its Applications*, 2nd ed., 522 pp., John Wiley, New York, 1973.

Steig, E. J., J. L. Fastook, C. Zweck, I. D. Goodwin, K. J. Licht, J. W. C. White, and R. P. Ackert, West Antarctic ice sheet elevation changes, in *The West Antarctic Ice Sheet: Behavior and Environment, Antarctic Res. Ser.*, vol. 77, edited by R. B. Alley and R. A. Bindschadler, pp. 75–90, AGU, Washington, D. C., 2001.

Tamisiea, M. E., J. X. Mitrovica, G. A. Milne, and J. L. Davis, Global geoid and sea level changes due to present-day ice mass fluctuations, *J. Geophys. Res.*, *106*, 30,849–30,863, 2001.

Trupin, A., and C. K. Shum, Determination of mass balance of polar ice from gravity, in *I.A.G. Symposia 123: Gravity, Geoid and Geodynamics 2000*, edited by M. G. Sideris, pp. 367–372, Springer-Verlag, New York, 2001.

Tushingham, A. M., and W. R. Peltier, Ice-3G: A new global model of late Pleistocene deglaciation based upon geophysical predictions of postglacial relative sea level change, *J. Geophys. Res.*, *96*, 4497–4523, 1991.

Velicogna, I., and J. M. Wahr, Postglacial rebound and Earth's viscosity structure from GRACE, *J. Geophys. Res.*, *107*, doi:10.1020/2001JB001735, in press, 2002.

Velicogna, I., J. M. Wahr, and H. V. den Dool, Can surface pressure be used to remove atmospheric contributions from GRACE data with sufficient accuracy to recover hydrological signals?, *J. Geophys. Res.*, *106*, 16,415–16,434, 2001.

Vermeersen, L. L. A., and R. Sabadini, A new class of stratified viscoelastic models by analytical techniques, *Geophys. J. Int.*, *129*, 531–570, 1997.

Wahr, J. M., D. Han, and A. Trupin, Prediction of vertical uplift caused by changing polar ice volumes on a viscoelastic Earth, *Geophys. Res. Lett.*, *22*, 977–980, 1995.

Wahr, J. M., M. Molenaar, and F. Bryan, Time variability of the Earth's gravity field: Hydrological and oceanic effects and their possible detection using GRACE, *J. Geophys. Res.*, *103*, 30,205–30,229, 1998.

Wahr, J., D. Wingham, and C. Bentley, A method of combining ICESat and

GRACE satellite data to constrain Antarctic mass balance, *J. Geophys. Res.*, *105*, 16,279–16,294, 2000.

Wang, P., and X. Wu, OpenMP programming for a global inverse model, *J. Sci. Programming*, in press, 2002.

Wingham, D. J., A. J. Ridout, R. Scharroo, R. J. Arthern, and C. K. Shum, Antarctic elevation change from 1992 to 1996, *Science*, *282*, 456–458, 1998.

Wu, P., and W. R. Peltier, Glacial isostatic adjustment and the free air gravity anomaly as a constraint on deep mantle viscosity, *Geophys. J. R. Astron. Soc.*, *74*, 377–449, 1983.

Yoder, C. F., J. G. Williams, J. O. Dickey, B. E. Schutz, R. J. Eanes, and B. D. Tapley, Secular variation of Earth's gravitational harmonic J_2 coefficient from LAGEOS and nontidal acceleration of Earth rotation, *Nature*, *303*, 757–762, 1983.

E. R. Ivins, R. Kwok, P. Wang, M. M. Watkins, and X. Wu, Jet Propulsion Laboratory, California Institute of Technology, 4800 Oak Grove Dr., MS 238/600, Pasadena, CA 91109, USA. (eri@scn1.jpl.nasa.gov; ron@radar-sci.jpl.nasa.gov; wangp@azalea.jpl.nasa.gov; mmw@cobra.jpl.nasa.gov; Xiaoping.Wu@jpl.nasa.gov)

J. M. Wahr, Department of Physics and CIRES, University of Colorado, Boulder, CO 80309-0390, USA. (wahr@longo.colorado.edu)

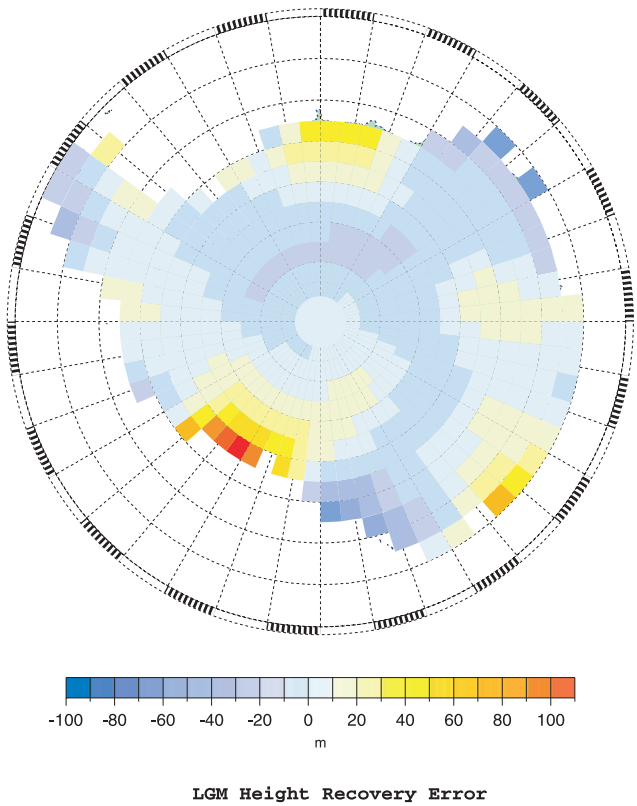

Figure 2. The 450-km Gaussian average inverse recovery errors in the LGM heights over Antarctica. Elevation rate noise is assumed to be 1.5 mm/yr over each grid for 5 years of GLAS altimeter measurements.

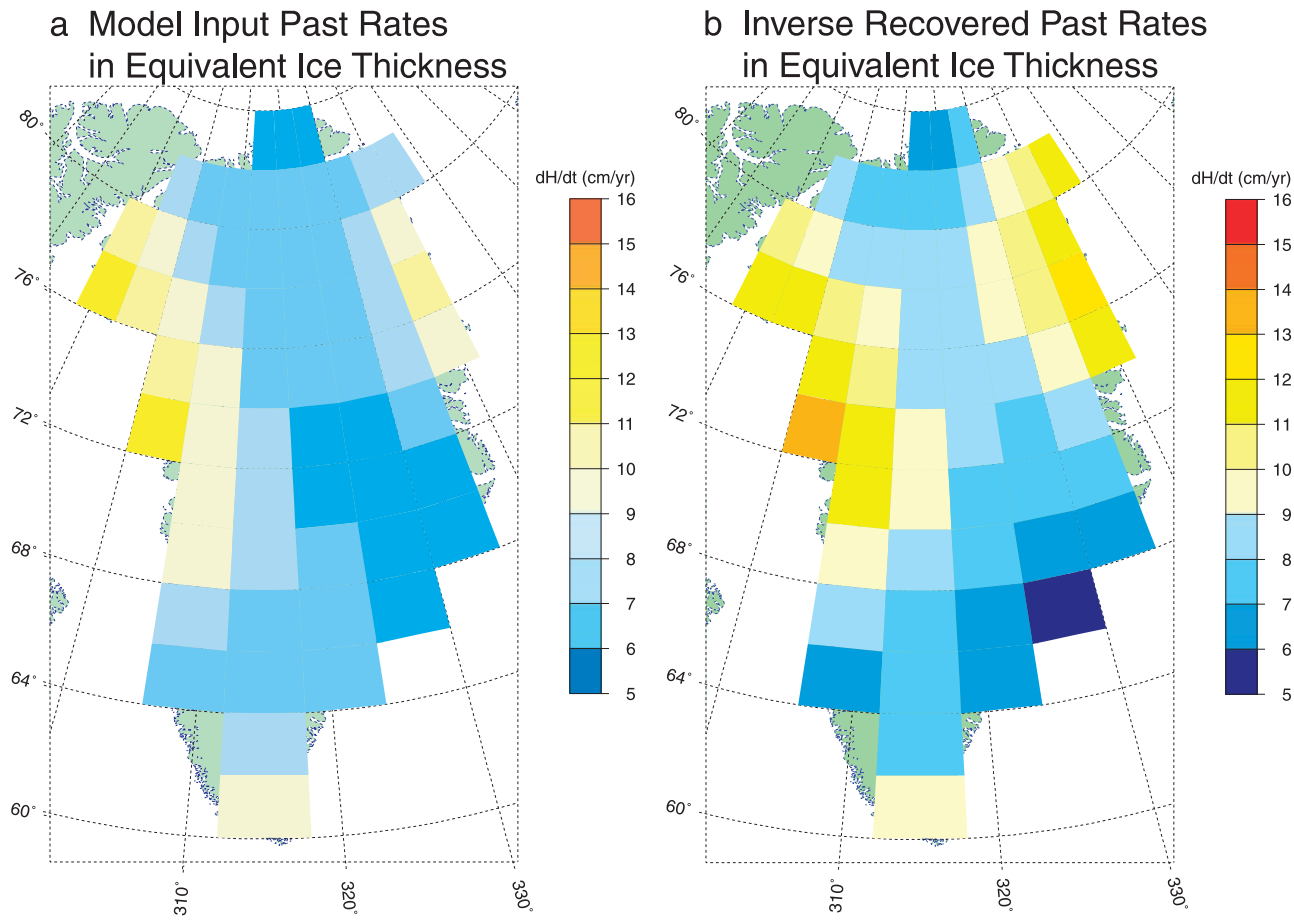

Figure 3. (a) Simulation input model and (b) inverse recovered past trends in Greenland. Both are 450-km Gaussian averaged; 7 mm/yr altimeter elevation rate noise is assumed to reflect instrument and possible spatially variable compaction errors.

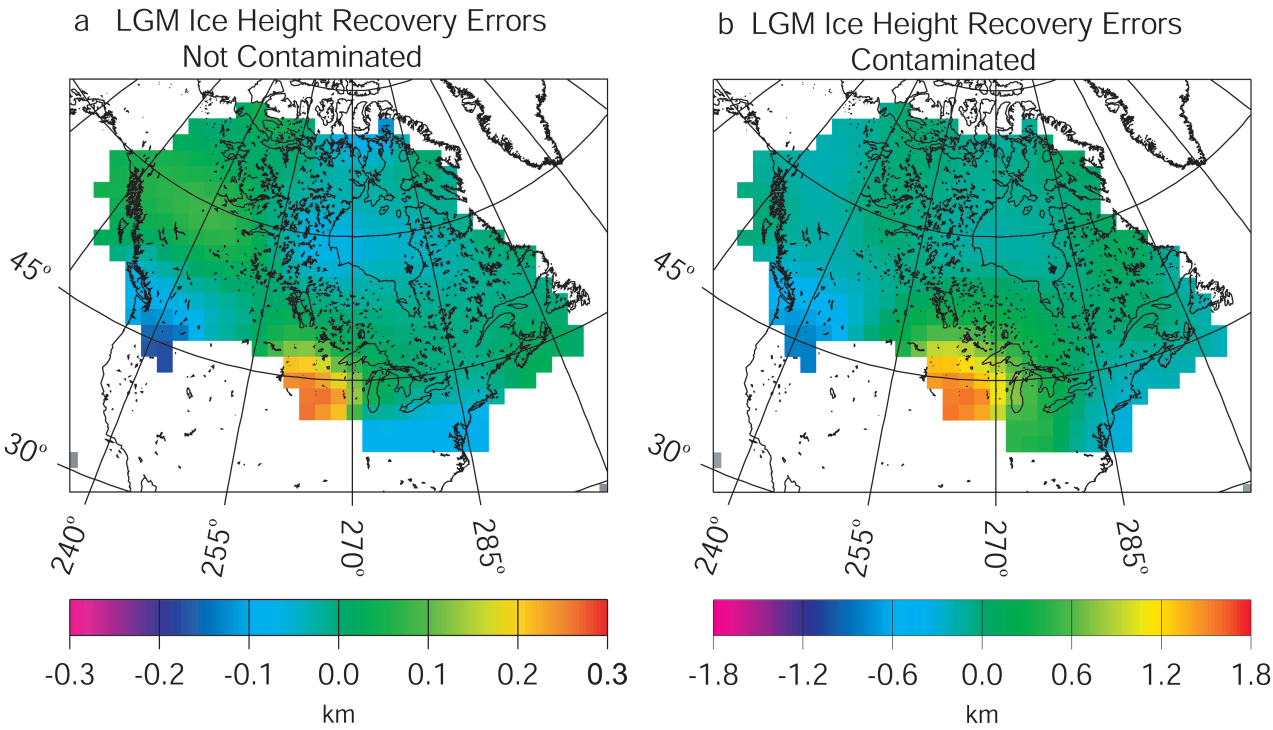

Figure 4. The 450-km Gaussian average inverse recovery errors in the LGM ice heights over the ancient Laurentian ice sheet. (a) Simulated data that do not include hydrological noise from the area once covered by the ice sheet and deglaciation times are assumed known and (b) data that include hydrological noise from the area and deglaciation times are also solved for with a priori uncertainty of 5 kyr for each grid.